

Multichannel Quantum Defect Theory for cold molecular collisions with a strongly anisotropic potential energy surface

James F. E. Croft and Jeremy M. Hutson

*Joint Quantum Centre (JQC) Durham/Newcastle, Department of Chemistry,
Durham University, South Road, Durham, DH1 3LE, United Kingdom*

(Dated: October 29, 2018)

We show that multichannel quantum defect theory (MQDT) can be applied successfully as an efficient computational method for cold molecular collisions in Li+NH, which has a deep and strongly anisotropic interaction potential. In this strongly coupled system, closed-channel poles restrict the range over which the MQDT \mathbf{Y} can be interpolated. We present an improved procedure to transform the MQDT reference functions so that the poles are removed from the energy range of interest. Effects due to very long-range spin-dipolar couplings are outside the scope of MQDT, but can be added perturbatively. The new procedure makes it possible to calculate the elastic and inelastic cross sections needed to evaluate the feasibility of sympathetic cooling of NH by Li using coupled-channel calculations at only 5 combinations of energy and field.

I. INTRODUCTION

Cold and ultracold molecules provide an exciting doorway to new fields in physics and chemistry. They share the controllability and tunable interactions that have made cold atom studies so fruitful. However, the richer structure of molecules makes them suitable for many new applications and research directions [1, 2]. Polar molecules are of particular interest because their electric dipole moment allows the interactions between them to be controlled and manipulated by external fields. This strong tunable response may make it possible to develop a fully controlled chemistry [3] where every degree of freedom of the reaction can be tuned, providing fundamental insights into chemical reaction processes. Molecules such as KRb [4] and Cs₂ [5] have already been produced at submicrokelvin temperatures in their lowest-energy electronic, vibrational, rotational, and hyperfine state, by magnetoassociation followed by laser state transfer. Reactions of ultracold ⁴⁰K⁸⁷Rb with itself and with K and Rb atoms have been studied [6], and it was seen that quantum statistics and quantum threshold laws play an important role in determining the rates of inelastic collisions.

The only ultracold molecules that are accessible with current methods are alkali-metal dimers. However, there is great interest in producing samples of other molecular species in the ultracold regime. The most promising route to this is first to cool and trap them in the cold regime (at temperatures below 1 K), using a method such as buffer-gas cooling [7] or molecular beam deceleration [8] and then to bring them to the ultracold regime using a second-stage approach such as evaporative cooling [9], sympathetic cooling [10], or laser cooling [11, 12].

Evaporative and sympathetic cooling both rely on elastic collisions to thermalize the sample, but both can be prevented by inelastic collisions that release kinetic energy and lead to trap loss. Collisional properties are also key to methods for *controlling* ultracold atoms and molecules. Calculations on atomic and molecular collisions

are therefore crucial to both the production and control of cold and ultracold molecules. Such calculations require the solution of the set of coupled differential equations obtained from the Schrödinger equation. There are various numerical methods for solving these coupled differential equations, of which the most commonly used is the full coupled-channels method. This propagates the matrix solution of the Schrödinger equation from short to long range and takes a time proportional to N^3 , where N is the number of coupled channels. The properties of completed collisions are described by the scattering matrix \mathbf{S} , which is obtained by matching the propagated solutions to free-particle wavefunctions (Ricatti-Bessel functions) at long range [13].

Full coupled-channels calculations can be extremely expensive, particularly in applied electric and magnetic fields [14–16]. The expense is particularly great for systems with deep and strongly anisotropic potential wells [17], for molecule-molecule collisions [18], or when nuclear hyperfine interactions are included [19, 20].

In cold collision studies, the scattering \mathbf{S} matrix is often a fast function of collision energy E and magnetic field B , with extensive structure due to scattering resonances and discontinuous behavior at threshold. Calculations are thus required over a fine grid of energies and/or applied field, typically over an energy range of order 1 K, from threshold, and for magnetic fields up to a few thousand G. This contrasts with the situation for collisions of ultracold atoms, where the energy range of interest is commonly a few μ K and the fields are typically a few hundred G.

Approaches based on multichannel quantum defect theory (MQDT) avoid the repetition of the expensive propagation by representing the scattering properties in terms of a matrix $\mathbf{Y}(E, B)$ that is a smooth function of E and B [21–25]. MQDT has proved highly successful for cold atomic interactions [24–30], and more recently it has been applied to collisions of cold and ultracold molecules [31–36]. MQDT defines the matrix $\mathbf{Y}(E, B)$ at a matching distance, r_{match} , at relatively short range in order to achieve this insensitivity to energy and field. The \mathbf{Y} ma-

trix contains all the scattering dynamics inside r_{match} . The smooth variation of \mathbf{Y} allows it to be obtained once and then used for calculations over a wide range of energies and fields, or obtained by interpolation from a few points. The computational cost of calculations at additional energies and fields is only proportional to N , not N^3 .

We have previously demonstrated the application of MQDT to cold molecular collisions for the moderately anisotropic system Mg+NH($^3\Sigma^-$) [34, 36]. In ref. [36], we showed that the choice made for the *phase* of the MQDT reference functions is very important in producing a \mathbf{Y} matrix that can be interpolated smoothly over a wide range of energy and field. The purpose of the present paper is to explore how the approach performs for a much more strongly anisotropic system with many more closed channels. For this purpose we choose Li+NH, which has been studied previously using full coupled-channels calculations by Wallis *et al.* [17]. As in ref. [17], we focus on collisions between spin-polarized Li and NH, which occur on the quartet potential energy surface. This surface is deep and highly anisotropic, with a well depth about 1800 cm^{-1} at the Li-NH geometry but only 113 cm^{-1} at the NH-Li geometry. With a small but important modification to the method of choosing phases described in ref. [36], we find that we can obtain accurate results for elastic and inelastic cross section, over the entire range of energies relevant to sympathetic cooling, using only 5 coupled-channels calculations.

II. THEORY

The theory of MQDT is given in details in refs. [22–25]. Here we give only a brief description, following references [34, 36], which is sufficient to describe the notation we use.

MQDT makes the approximation that the multichannel Schrödinger equation is uncoupled at distances $r > r_{\text{match}}$, so that its solution in this region may be written in the matrix form

$$\boldsymbol{\Psi} = r^{-1} [\mathbf{f}(r) + \mathbf{g}(r)\mathbf{Y}]. \quad (1)$$

Here \mathbf{f} and \mathbf{g} are diagonal matrices containing the functions f_i and g_i , which are linearly independent solutions of a reference Schrödinger equation in each asymptotic channel i ,

$$\left[-\frac{\hbar^2}{2\mu} \frac{d^2}{dr^2} + U_i^{\text{ref}}(r) - E \right] f_i(r) = 0, \quad (2)$$

and similarly for $g_i(r)$. μ is the reduced mass, and the reference potentials $U_i^{\text{ref}}(r)$ approach the true potential at long range. They include the centrifugal terms $\hbar^2 L_i(L_i+1)/2\mu r^2$, where L_i is the partial-wave quantum number for channel i .

The phase of the short-range reference functions f_i and g_i is a disposable parameter of MQDT and may be chosen to generate a \mathbf{Y} matrix that is smooth and pole-free

over a wide range of energy and field [36]. Equation (1) shows that the \mathbf{Y} matrix has a pole whenever the component of the propagated multichannel wavefunction ψ_i in any channel i is proportional to the reference function g_i and has no contribution from f_i , i.e. when g_i and the full coupled-channels solution have the same phase at r_{match} . In ref. [36], we proposed transforming the pair of reference functions f_i and g_i in channel i with a rotation angle θ_i , chosen so that the diagonal matrix elements Y_{ii} is 0 at a particular reference energy E_{ref} and field B_{ref} . This ensures that the reference function g_i and the full coupled-channels solution in channel i are perfectly out of phase at the chosen r_{match} , and the resulting \mathbf{Y} matrix is therefore pole-free close to E_{ref} and B_{ref} [36].

The range of the pole-free region is dependent on where the matching occurs. When matching is in the classically allowed region, the phases of both the reference functions and the propagated coupled-channels solutions vary approximately linearly with energy and setting the diagonal \mathbf{Y} matrix elements to zero is effective: the *relative* phase of the reference functions and the coupled-channels solution is a slow function of energy. For a closed channel where matching is carried out in the classically forbidden region, however, there is resonance structure in both the coupled-channels solutions and the reference functions so that the phase of each is a fast (and nonlinear) function of energy. Fortunately, the energies at which the resonance structure occurs depend on the choice of θ_i . In the present work we show that a more sophisticated choice of θ_i than that of ref. [36] can produce a larger pole-free region for closed channels.

A. Basis set and quantum numbers

We construct the collision Hamiltonian in the fully uncoupled basis set $|nm_n\rangle|s_{\text{NH}}m_{s_{\text{NH}}}\rangle|s_{\text{Li}}m_{s_{\text{Li}}}\rangle|LM_L\rangle$, where the quantum numbers n and s_{NH} describe the rotation and electron spin of the NH molecule and s_{Li} describes the electron spin of the Li atom. The corresponding m quantum numbers are the projections onto the space-fixed magnetic field axis. Hyperfine structure is neglected. The matrix elements required for the coupled equations are the same as for scattering of NH from a closed-shell atom [16], with the addition of the anisotropic intermolecular spin-spin dipolar interaction [17].

The coupled-channels calculations may in principle be carried out in any sufficiently complete basis set. However, the \mathbf{Y} and \mathbf{S} matrices are expressed in a basis set of eigenfunctions of the field-dressed monomer Hamiltonians. At low field the states of the NH molecule are approximately described by quantum numbers j and m_j , where j is the resultant of n and s . We label elements of \mathbf{Y} and \mathbf{S} by subscripts $n, j, m_j, m_{s_{\text{Li}}}, L, M_L \rightarrow n', j', m'_j, m'_{s_{\text{Li}}}, L', M'_L$. For diagonal elements we suppress the second set of labels.

B. Numerical methods

The coupled-channels calculations required for both MQDT and the full coupled-channels approach are carried out using the MOLSCAT package [37], as modified to handle collisions in magnetic fields [16]. The coupled equations are solved numerically using the hybrid log-derivative propagator of Alexander and Manolopoulos [38], which uses a fixed-step-size log-derivative propagator in the short-range region ($r_{\min} \leq r < r_{\text{mid}}$) and a variable-step-size Airy propagator in the long-range region ($r_{\text{mid}} \leq r \leq r_{\text{max}}$). As in ref. [17], the full coupled-channels calculations use $r_{\min} = 1.8 \text{ \AA}$, $r_{\text{mid}} = 12.5 \text{ \AA}$ and $r_{\text{max}} = 600 \text{ \AA}$ (where $1 \text{ \AA} = 10^{-10} \text{ m}$). MQDT requires coupled-channels calculations only from r_{\min} to r_{match} (which is less than r_{mid}), so only the fixed-step-size propagator is used in this case.

The initial MQDT reference functions and quantum defect parameters are obtained as described in ref. [34], using the renormalized Numerov method [39] to solve the 1-dimension Schrödinger equations for the reference potentials. In this paper all MQDT calculations use the reference potential

$$U_i^{\text{ref}}(r) = V_0(r) + \frac{\hbar^2 L_i(L_i + 1)}{2\mu r^2} + E_i^\infty, \quad (3)$$

where $V_0(r)$ is the isotropic part of the interaction potential and L_i is the partial-wave quantum number for channel i . The reference potential contains a hard wall at $r = r_i^{\text{wall}}$, so that $U_i^{\text{ref}}(r) = \infty$ for $r < r_i^{\text{wall}}$. In the present paper we choose $r_i^{\text{wall}} = 4.0 \text{ \AA}$. This reference potential has been shown to produce quantitatively accurate results for Mg+NH [34, 36].

The uncoupled basis functions used to solve the coupled-channel equations are not eigenfunctions of the Hamiltonians of the separated monomers. The log-derivative matrix obtained from the coupled-channel calculations at a distance r_{match} is therefore transformed into a basis set that diagonalizes the asymptotic Hamiltonian [40]. The MQDT \mathbf{Y} matrix is then obtained by matching to this log-derivative matrix at r_{match} using Eq. (13) of ref. [34]. All channels with $n \geq 2$ are treated as strongly closed and thus not included in the MQDT part of the calculation, but are included in the log-derivative propagation.

III. RESULTS AND DISCUSSION

In a magnetic field, the lowest Li-NH threshold ($n = 0$, $s_{\text{NH}} = 1$, $s_{\text{Li}} = \frac{1}{2}$) splits into 6 Zeeman sublevels. We consider collisions between Li atoms and NH molecules that are both initially in their magnetically trappable low-spin-seeking states, $m_{s,\text{Li}} = +1/2$ and $m_{s,\text{NH}} = +1$. This corresponds to the highest of the 6 thresholds.

Figure 1 shows the variation of the representative element $Y_{1,2,-2,-\frac{1}{2},7,4}$, as a function of the matching distance and energy, when the phases θ_i are chosen to make

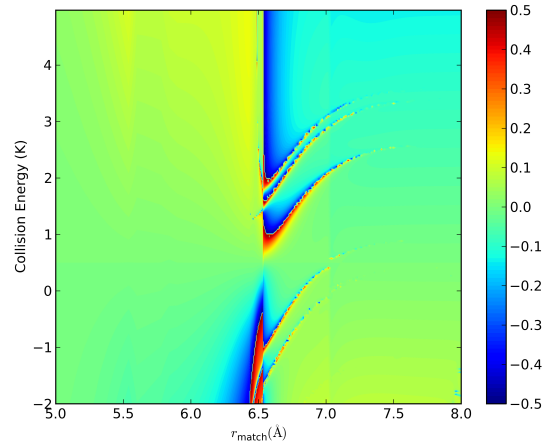


FIG. 1. (Color online) $\arctan Y_{ii}/\pi$ for a single representative diagonal \mathbf{Y} matrix element, as a function of collision energy E and r_{match} , with the phases θ_i set so that $Y_{ii} = 0$ in all channels for energy $E_{\text{ref}} = 0.5 \text{ K}$ and field $B_{\text{ref}} = 10 \text{ G}$.

all diagonal \mathbf{Y} matrix elements zero at collision energy $E_{\text{ref}} = 0.5 \text{ K}$ and field $B_{\text{ref}} = 10 \text{ G}$. It may be seen that there are poles (where $\arctan Y_{ii}/\pi$ passes through $\pm 1/2$) whose positions depend strongly on r_{match} . Other \mathbf{Y} matrix elements are quantitatively different but have poles in the same places. The basis set used for Figure 1 includes all functions up to $n_{\text{max}} = 3$ and $L_{\text{max}} = 8$. This unconverged basis set was used due to the substantial computational cost of performing a full coupled-channels calculation at every energy in the Figure. The outer turning point of the $n = 1$ reference potential is at 6.1 \AA , and it may be seen that, for values of r_{match} inside this, the \mathbf{Y} matrix is pole-free over many K. However, MQDT with such small values of r_{match} does not produce accurate results because it neglects all channel couplings that exist outside r_{match} . When $r_{\text{match}} > 6.1 \text{ \AA}$, poles start to enter the \mathbf{Y} matrix in the energy range of interest. As r_{match} increases further, the poles move and at some values of r_{match} can come within 0.1 K of E_{ref} .

A contour plot such as Fig. 1 requires coupled-channels calculations at every energy, and producing it thus sacrifices most of the computational savings that MQDT is designed to achieve. In addition, we need a procedure for choosing the phases θ_i that will guarantee a large pole-free region for *any* choice of r_{match} . In the remainder of this paper, we perform calculations at only a single value of $r_{\text{match}} = 6.5 \text{ \AA}$, deliberately chosen to be in a region where Fig. 1 shows that there are poles in \mathbf{Y} inconveniently close to E_{ref} . In addition, the remaining calculations use a basis set including all functions up to $n_{\text{max}} = 6$ and $L_{\text{max}} = 8$, except where stated otherwise.

The dependence of a diagonal \mathbf{Y} matrix element on the phase of the reference functions (in any channel handled by MQDT) is

$$Y_{ii}(E) = \tan[\theta_i + \delta_i(E)], \quad (4)$$

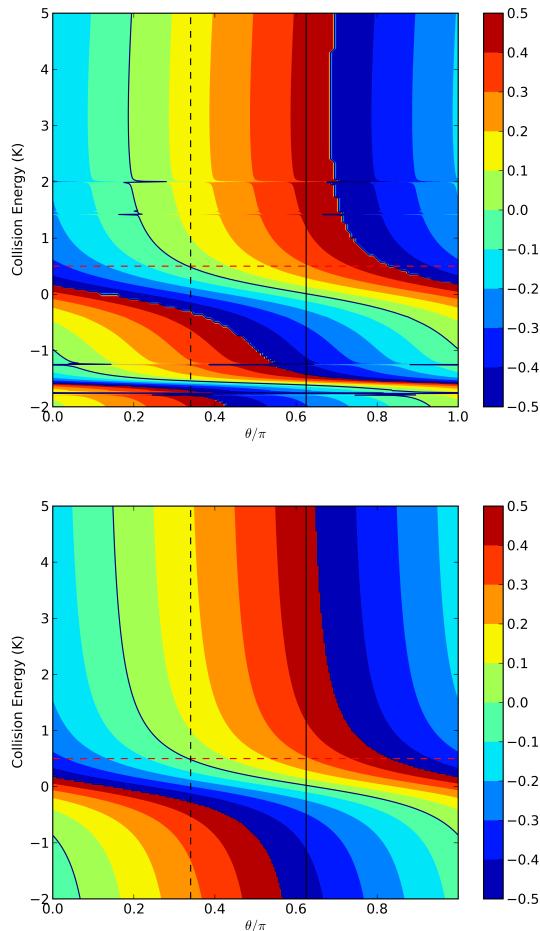


FIG. 2. (Color online) Upper panel: $\arctan Y_{ii}/\pi$ from coupled-channels calculations at $B = 10$ G for a single diagonal element, $Y_{1,2,-2,-\frac{1}{2},7,4}$, with $\theta_{i'}$ set so that $Y_{i'i'} = 0$ in all other channels i' at $E_{\text{ref}} = 0.5$ K (horizontal dashed line). Lower panel: $\arctan Y_{ii}/\pi$ as a function of energy and θ_i for a single uncoupled channel as given by Eqs. (4) and (5).

where $\delta_i(E)$ is the phase shift between the unrotated reference function f_i and the propagated multichannel wavefunction in channel i . For a closed channel that is capable of supporting resonances, the phase shift around a resonance has a Breit-Wigner form,

$$\delta_i(E) = \bar{\delta}_i(E) + \arctan\left(\frac{\Gamma_i/2}{E - E_i^{\text{res}}}\right), \quad (5)$$

where $\bar{\delta}_i$ is a slowly varying (non-resonant) background term. The resonant part of this function is shown in the lower panel of Fig. 2, for values of the parameters appropriate to one of the channels in Li+NH. It may be seen that choosing a value of θ_i that makes Y_{ii} zero (shown by the dashed vertical line) does not guarantee a large pole-free region in the case where E_{ref} is close to E_i^{res} . A much better choice in this case is to set θ_i to the value shown by the solid vertical line. In the following

we will show how this can be achieved.

A basic problem of MQDT in coupled-channel problems is that a pole in \mathbf{Y} that originates in *any* channel causes a pole in *every* channel. We refer to this as the *contamination* of one channel by another. The upper panel of Figure 2 shows $\arctan Y_{ii}/\pi$ for the single matrix element, $Y_{1,2,-2,-\frac{1}{2},7,4}$, obtained from coupled-channels calculations as a function of θ_i and collision energy E . The phases $\theta_{i'}$ in all other channels i' are set to the values that produce $Y_{i'i'} = 0$ at $E_{\text{ref}} = 0.5$ K. The broad horizontal sweep around 0 K arises from a resonance in channel i , while the narrower sweeps at -1.8 K, -1.6 K, -1.2 K, 1.4 K and 2.0 K are poles due to contamination from other channels. Setting $Y_{i'i'}$ to zero in all these other channels has shifted these contamination effects to energies either above about 1.4 K or below -1.2 K, leaving a region of about 2.6 K uncontaminated by other channels. For the specific circumstances shown in Figure 2, it is seen that choosing θ_i so that $Y_{ii} = 0$ results in $\theta_i/\pi \approx 0.33$ (dashed vertical line). This produces a pole in Y_{ii} itself at about -0.1 K, which is inconveniently close to E_{ref} . However, a choice of $\theta_i/\pi = 0.63$ (solid vertical line) would produce a much larger pole-free region, limited only by poles due to contamination effects in other channels. If improved values of $\theta_{i'}$ can also be obtained for these contamination poles, then there is clearly the prospect of achieving a much improved pole-free region.

The pole structure in channel i when uncontaminated by other channels is given by Eqs. (4) and (5). In order to use these to obtain a better choice of θ_i , we need values for E_i^{res} , Γ_i and $\bar{\delta}_i$. To obtain these we first optimize the phases as in ref. [36], transforming the reference functions so that $Y_{ii} = 0$ in all channels at energy E_{ref} . This provides at least a small region where Y_{ii} is uncontaminated by poles in other channels. We then carry out coupled-channels calculations at 2 additional energies near E_{ref} , and use Eqs. (4) and (5) to obtain the three parameters E_i^{res} , Γ_i and $\bar{\delta}_i$ numerically, neglecting the slow variation of $\bar{\delta}_i$ with E . The optimum pole-free region for this channel is then achieved by setting $\theta_i = \pi/2 - \bar{\delta}_i$.

The pole-free region for the entire \mathbf{Y} matrix is optimized by applying this procedure in all channels where there is resonant structure close to the reference energy. We first calculate the numerical second derivative of the diagonal matrix elements Y_{ii} with respect to energy. We then select the channel with the largest second derivative, apply the procedure described above, and use the new set of phases to recalculate the three \mathbf{Y} matrices. Because of channel mixing, this in principle changes *all* the diagonal matrix elements. If it reduces $\sum_i |d^2 Y_{ii}/dE^2|$ then we accept the new value of θ_i . If not, we move on to the next channel and apply the same procedure. We loop over the channels in this manner until there is no channel for which changing θ_i to $\pi/2 - \bar{\delta}_i$ reduces $\sum_i |d^2 Y_{ii}/dE^2|$. This is an inexpensive procedure, as it uses the same 3 coupled-channels calculations as before. Only the closed channels need to be included in the loop since only these channels have resonance structure.

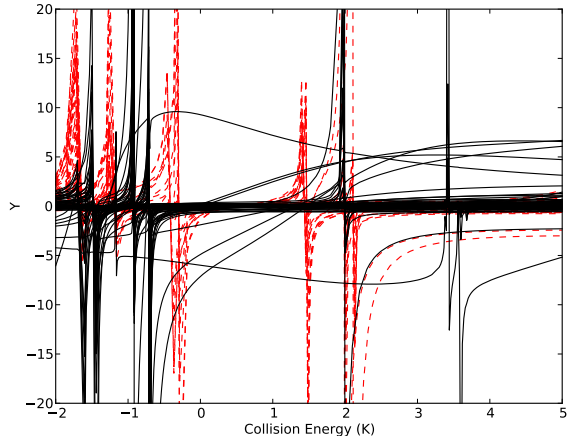


FIG. 3. (Color online) Y_{ii} as a function of energy for all channels, with all phases θ_i optimized as described in ref. [34] (dashed red lines) or using Eqs. (4) and (5) (solid black lines). In both cases the phases are optimized at $r_{\text{match}} = 6.5 \text{ \AA}$ for $E_{\text{ref}} = 0.5 \text{ K}$ and $B_{\text{ref}} = 10 \text{ G}$.

Figure 3 compares the final matrix elements Y_{ii} in all the channels included in the MQDT procedure, obtained with the two optimization schemes. The dashed red lines show the result of choosing θ_i so that Y_{ii} is zero in every channel, as in ref. [36], while the solid black lines show the result of optimizing θ_i as described above. Both calculations use $r_{\text{match}} = 6.5 \text{ \AA}$ and optimize θ_i at $E_{\text{ref}} = 0.5 \text{ K}$ and $B_{\text{ref}} = 10 \text{ G}$. It may be seen that taking account of closed-channel resonances significantly increases the pole-free range of \mathbf{Y} . Furthermore, it produces \mathbf{Y} matrix elements that are considerably more linear between 0 and 1 K and may thus be interpolated more accurately.

Figure 4 compares diagonal T-matrix elements $|T_{ii}|^2$ (where $T_{ij} = \delta_{ij} - S_{ij}$) obtained from full coupled-channels calculations with those from the MQDT method using interpolation. The MQDT results were obtained by interpolating (and extrapolating) \mathbf{Y} quadratically using 3 points separated by 0.1 K around 0.5 K. The MQDT results obtained by interpolation are very similar to the full coupled-channels results, even around the resonance features at $E \approx 0.7 \text{ K}$.

IV. APPLICATION TO SYMPATHETIC COOLING

The key quantity that determines whether sympathetic cooling can succeed is the ratio γ of elastic to inelastic cross sections for collisions of trapped molecules with coolant atoms. This ratio typically needs to be greater than about 100 if trapped molecules are to undergo enough elastic (thermalizing) collisions to achieve cooling before undergoing an inelastic collision that releases kinetic energy and causes trap loss. Wallis *et al.* [17] have investigated Li + NH collisions using coupled-channel

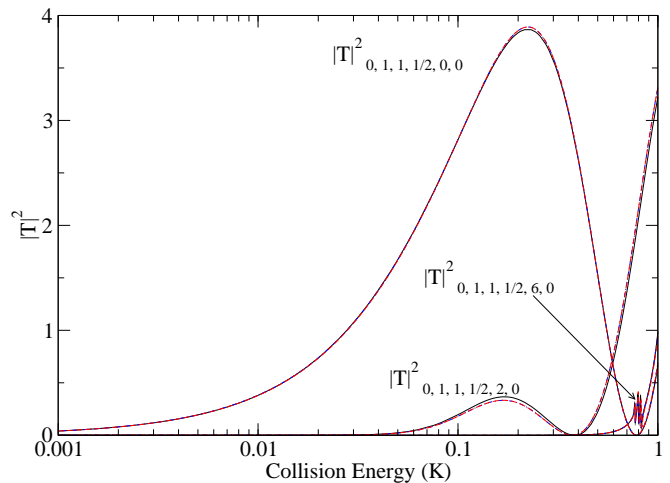


FIG. 4. (Color online) Squares of diagonal T-matrix elements T_{m_j, L, M_L} in the incoming channels for $m_j = +1$ and $L = 0, 2$ and 6 at $B = 10 \text{ G}$, obtained from full coupled-channels calculations (solid, black) and MQDT using optimized reference functions for $r_{\text{match}} = 6.5 \text{ \AA}$ both with (dot-dash, blue) and without (dashed, red) interpolation. $L = 4$ is not shown because it obscures the resonant feature for $L = 6$.

calculations, and produced contour plots that show the ratio γ as a function of collision energy E and magnetic field B . These calculations were very expensive because they required calculations on a fine grid of energies and fields. The contour plots given in ref. [17] actually included coupled-channel calculations at 204 combinations of energy and field.

MQDT offers the possibility of producing the entire contour plot from coupled-channels calculations at just three energies (required to optimize the phases) and two magnetic fields. We have therefore used MQDT to repeat the calculations of ref. [17] on the unscaled potential energy surface. Coupled-channel calculations from r_{min} to r_{match} were carried out at collision energies $E = 0.01, 0.05$ and 0.1 K at magnetic field $B = 10 \text{ G}$ to optimize the phases, and at $E = 0.01$ and 0.1 K at $B = 1000 \text{ G}$ to allow linear interpolation in B and E . These calculations used a basis set with $n_{\text{max}} = 6$ and $L_{\text{max}} = 8$ to allow direct comparison with ref. [17]. The resulting contour plot of γ is compared with the results of ref. [17] in the upper panel of Figure 5: it may be seen that there is good agreement at both high collision energies ($E > 0.01 \text{ K}$) and high fields ($B > 100 \text{ G}$), but that MQDT by itself breaks down when both E and B are small [41].

The inaccuracy in MQDT at low energy and low field occurs because, in this region, the inelastic cross sections are dominated by *long-range* inelasticity involving the magnetic dipole interaction between the spins of Li and NH. As described by Janssen *et al.* [18], there are long-range avoided crossings between the effective potential curves for the incoming channel and for inelastic channels with larger values of L . These crossings usually occur *outside* the centrifugal barriers, and even coupled-channel

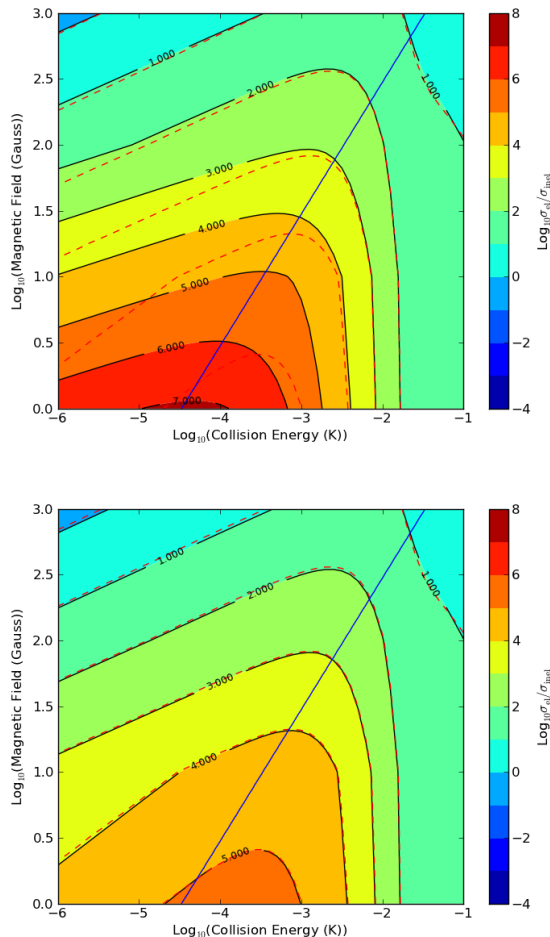


FIG. 5. (Color online) Contour plots of the ratio γ of elastic to inelastic cross sections for Li+NH collisions as a function of energy and magnetic field, obtained using a basis set with $n_{\max} = 6$ and $L_{\max} = 8$. The solid contours and shading show the MQDT results and the dashed contours show the results from full coupled-channel calculations [17]. The diagonal blue lines show the field at which the Zeeman energy in a quadrupole trap is $6k_B T$. Upper panel: results from MQDT alone. Lower panel: results from MQDT with long-range spin-spin couplings added using the hybrid Born approach.

calculations must be propagated to very long range (hundreds of Å) to capture their effects. They are thus outside the scope of MQDT, which neglects couplings outside r_{match} .

The long-range couplings may however be included perturbatively at very little expense. Janssen *et al.* [42] have developed both a simple Born approximation and a distorted-wave Born approximation (DWBA) for calculating the inelastic cross sections due to these long-range couplings. The simple Born approximation is stable to evaluate, but can give results up to a factor of 2 in error for cross sections for initial $L = 0$ because it does not take account of the phase shift due to short-range

interactions. The DWBA, by contrast, is quite accurate for initial $L = 0$ but can be unstable when L and L' are both non-zero. However, in the latter case, short-range effects are unimportant. We have therefore used a hybrid Born approximation, made up of the DWBA for initial $L = 0$ and the simple Born approximation for initial $L > 0$. When we add the resulting inelastic cross sections to those from MQDT, we obtain the contour plot for the ratio γ shown in the lower panel of Figure 5. It may be seen that this gives essentially complete agreement with the full coupled-channel results.

The MQDT approach makes it feasible to use a larger basis than was possible in ref. [17] and to carry out the calculations on a much finer grid of energies and fields. Figure 6 shows the results obtained from MQDT with perturbative long-range corrections for a converged basis set with $n_{\max} = 10$ and $L_{\max} = 8$, with cross sections calculated on a 51×51 grid of energies and fields. The resulting coupled-channels basis sets contains 1887 basis functions, as compared to 937 functions for the smaller basis set used in Figure 5, and each coupled-channel calculation is therefore a factor of 8 more expensive.

As described in ref. [17], the elastic and inelastic cross sections are a strong function of both potential scaling and basis set size, because they depend sensitively on the positions of near-dissociation levels. Because of this, calculations on a single potential do not give quantitative predictions for the ratio of elastic and inelastic cross sections, and it is essential to explore the potential-dependence of the results. We found that using the unscaled potential with a converged basis set gave a highly atypical contour plot, because it has an accidentally near-zero scattering length and therefore a very small elastic cross section. The calculations in Figure 6 used a potential with an overall scaling factor of 0.995, which produces a much more typical contour plot. Exploring the dependence of the results on the scaling factor confirmed the conclusions of ref. [17], that sympathetic cooling of NH by Li is likely to succeed if the molecules can be precooled to a temperature around 20 mK.

V. CONCLUSIONS

We have demonstrated that Multichannel Quantum Defect Theory (MQDT) can provide quantitatively accurate cross sections for cold and ultracold elastic and inelastic collisions in magnetic fields for a strongly coupled molecular system, Li + NH. However, the choice of the phases of the MQDT reference functions is crucial. For Mg+NH, it was sufficient to choose the phases so that $Y_{ii} = 0$ in every channel included in MQDT [36]. For Li+NH, however, this does not guarantee that all closed-channel poles are moved far away in energy, and the poles can cause problems in interpolation. In the present paper, we have developed an improved approach for optimizing the phases that ensures that closed-channel poles are far away from a reference energy.

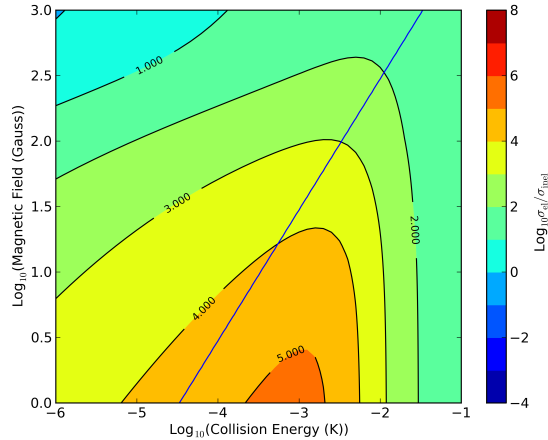


FIG. 6. (Color online) Contour plot of the ratio γ of elastic to inelastic cross sections for Li+NH collisions as a function of energy and magnetic field, obtained from MQDT calculations with perturbative long-range corrections, using a basis set with $n_{\max} = 10$ and $L_{\max} = 8$. The diagonal blue line shows the field at which the Zeeman energy in a quadrupole trap is $6k_B T$.

We have been able to reproduce the results of coupled-channel calculations across the entire range of energies and field relevant to sympathetic cooling of NH by Li, using our new version of MQDT combined with perturbative corrections for long-range inelasticity caused by the magnetic spin dipolar interaction. The MQDT results required coupled-channels calculations at only 5 combinations of energy and field, whereas the coupled-channels calculations [17] required 204 combinations. MQDT thus has enormous potential as an efficient computational method for molecular collisions.

VI. ACKNOWLEDGMENTS

We are grateful to Paul Julienne for many valuable discussions. JFEC is grateful to EPSRC for a High-End Computing Studentship. The authors are grateful for support from EPSRC and from EOARD Grant FA8655-10-1-3033.

-
- [1] L. D. Carr, D. DeMille, R. V. Krems, and J. Ye, *New J. Phys.* **11**, 055049 (2009).
- [2] G. Quémener and P. S. Julienne, *Chem. Rev.* **112**, 4949 (2012).
- [3] R. V. Krems, *Phys. Chem. Chem. Phys.* **10**, 4079 (2008).
- [4] K.-K. Ni, S. Ospelkaus, M. H. G. de Miranda, A. Pe'er, B. Neyenhuis, J. J. Zirbel, S. Kotochigova, P. S. Julienne, D. S. Jin, and J. Ye, *Science* **322**, 231 (2008).
- [5] J. G. Danzl, M. J. Mark, E. Haller, M. Gustavsson, R. Hart, J. Aldegunde, J. M. Hutson, and H.-C. Nägerl, *Nature Phys.* **6**, 265 (2010).
- [6] S. Ospelkaus, K.-K. Ni, D. Wang, M. H. G. de Miranda, B. Neyenhuis, G. Quémener, P. S. Julienne, J. L. Bohn, D. S. Jin, and J. Ye, *Science* **327**, 853 (2010).
- [7] J. Doyle, B. Friedrich, R. V. Krems, and F. Masnou-Seeuws, *Eur. Phys. J. D* **31**, 149 (2004).
- [8] H. L. Bethlem and G. Meijer, *Int. Rev. Phys. Chem.* **22**, 73 (2003).
- [9] B. K. Stuhl, M. T. Hummon, M. Yeo, G. Quémener, J. L. Bohn, and J. Ye, *Nature* **492**, 396 (2012).
- [10] P. Soldán and J. M. Hutson, *Phys. Rev. Lett.* **92**, 163202 (2004).
- [11] E. S. Shuman, J. F. Barry, and D. DeMille, *Nature* **467**, 820 (2010).
- [12] M. T. Hummon, M. Yeo, B. K. Stuhl, A. L. Collopy, Y. Xia, and J. Ye, arXiv, 1209.4069 (2012).
- [13] B. R. Johnson, *J. Comput. Phys.* **13**, 445 (1973).
- [14] A. Volpi and J. L. Bohn, *Phys. Rev. A* **65**, 052712 (2002).
- [15] R. V. Krems and A. Dalgarno, *J. Chem. Phys.* **120**, 2296 (2004).
- [16] M. L. González-Martínez and J. M. Hutson, *Phys. Rev. A* **75**, 022702 (2007).
- [17] A. O. G. Wallis, E. J. J. Longdon, P. S. Żuchowski, and J. M. Hutson, *Eur. Phys. J. D* **65**, 151 (2011).
- [18] L. M. C. Janssen, P. S. Żuchowski, A. van der Avoird, G. C. Groenenboom, and J. M. Hutson, *Phys. Rev. A* **83**, 022713 (2011).
- [19] M. Lara, J. L. Bohn, D. E. Potter, P. Soldán, and J. M. Hutson, *Phys. Rev. A* **75**, 012704 (2007).
- [20] M. L. González-Martínez and J. M. Hutson, *Phys. Rev. A* **84**, 052706 (2011).
- [21] C. H. Greene, U. Fano, and G. Strinati, *Phys. Rev. A* **19**, 1485 (1979).
- [22] C. H. Greene, A. R. P. Rau, and U. Fano, *Phys. Rev. A* **26**, 2441 (1982).
- [23] F. H. Mies, *J. Chem. Phys.* **80**, 2514 (1984).
- [24] F. H. Mies and M. Raoult, *Phys. Rev. A* **62**, 012708 (2000).
- [25] M. Raoult and F. H. Mies, *Phys. Rev. A* **70**, 012710 (2004).
- [26] B. Gao, *Phys. Rev. A* **78**, 012702 (2008).
- [27] P. S. Julienne, *Faraday Discuss.* **142**, 361 (2009).
- [28] B. Gao, *Phys. Rev. A* **58**, 4222 (1998).
- [29] P. S. Julienne and F. H. Mies, *J. Opt. Soc. Am. B* **6**, 2257 (1989).
- [30] J. P. Burke, J. L. Bohn, B. D. Esry, and C. H. Greene, *Phys. Rev. Lett.* **80**, 2097 (1998).
- [31] Z. Idziaszek and P. S. Julienne, *Phys. Rev. Lett.* **104**, 113202 (2010).
- [32] B. Gao, *Phys. Rev. Lett.* **105**, 263203 (2010).
- [33] Z. Idziaszek, G. Quémener, J. L. Bohn, and P. S. Julienne, *Phys. Rev. A* **82**, 020703 (2010).
- [34] J. F. E. Croft, A. O. G. Wallis, J. M. Hutson, and P. S. Julienne, *Phys. Rev. A* **84**, 042703 (2011).

- [35] M. Mayle, B. P. Ruzic, and J. L. Bohn, *Phys. Rev. A* **85**, 062712 (2012).
- [36] J. F. E. Croft, J. M. Hutson, and P. S. Julienne, *Phys. Rev. A* **86**, 022711 (2012).
- [37] J. M. Hutson and S. Green, “MOLSCAT computer program, version 14,” distributed by Collaborative Computational Project No. 6 of the UK Engineering and Physical Sciences Research Council (1994).
- [38] M. H. Alexander and D. E. Manolopoulos, *J. Chem. Phys.* **86**, 2044 (1987).
- [39] B. R. Johnson, *J. Chem. Phys.* **67**, 4086 (1977).
- [40] This transformation was neglected in refs. [34] and [36], where the partially coupled basis set used for the propagation was asymptotically very nearly diagonal. However, it is important in the decoupled basis set used here.
- [41] For consistency of comparison, we have performed MQDT calculations on the same grid of energies and fields as was used for the coupled-channels calculations in ref. [17] This actually included only 4 field values across the range shown. Including extra fields in the MQDT calculations produces small but visible changes in the contours.
- [42] L. M. C. Janssen, A. van der Avoird, and G. C. Groenenboom, *Eur. Phys. J. D* **65**, 177 (2011).